Variability of the nitric oxide nightglow at Venus during solar minimum

Emilie M. Royer, Franck Montmessin, Emmanuel Marcq

AGU PUBLICATIONS

JGR

Journal of Geophysical Research: Planets

RESEARCH ARTICLE
10.1002/2016JE005013

Key Points:
- We extracted the NO nightglow signal from a stellar occultation data set
- SPICAV imaging capabilities allow for a first quantification of the horizontal homogeneity of an airglow
- A long-term (≥ 30 years) permanent feature is observed at 2 A.M. solar local time south of the equator

Supporting Information:
- Supporting Information S1
- Figure S1
- Figure S2
- Figure S3

Correspondence to:
E. M. Royer,
emilie.royer@lasp.colorado.edu

Citation:
Royer, E. M., F. Montmessin, and E. Marcq (2016), Variability of the nitric oxide nightglow at Venus during solar minimum, *J. Geophys. Res. Planets*, *121*, 846–853, doi:10.1002/2016JE005013.

Received 10 FEB 2016
Accepted 26 APR 2016
Accepted article online 29 APR 2016
Published online 20 MAY 2016

Variability of the nitric oxide nightglow at Venus during solar minimum

E. M. Royer[1], F. Montmessin[2], and E. Marcq[2]

[1]LASP, University of Colorado Boulder, Boulder, Colorado, USA, [2]LATMOS, Guyancourt, France

Abstract We present results from a NO airglow inversion method based on Venus Express data acquired from 2006 to 2010, during the last solar minimum period. We retrieve an altitude of 114 ± 10 km for the emission peak of the NO layer, with an associated scale height of 20 ± 10 km and an average limb brightness of 59.3 kR with a standard deviation of 63 kR. The inversion method allows for the quantification of the horizontal homogeneity of the NO layer. Images of the SPICAV field of view show a great variability of airglow morphologies, with NO layers that can be horizontally homogenous and continuous over distances exceeding 100 km, as well as sporadic patches of NO on a smaller horizontal scale. Frequent secondary emissions seen at lower tangent altitudes are the signatures of the complex dynamics of the upper Venusian atmosphere.

1. Introduction

Above 100 km of altitude, in the mesosphere-thermosphere region of Venus, absorption of ultraviolet (UV) radiation is the main source of dissociation and ionization. On the dayside, molecules of CO_2 and N_2 are dissociated, leading to the formation of atomic nitrogen and oxygen. In this region of the atmosphere, the strong day/night temperature contrast allows the Subsolar/Antisolar (SSAS) circulation to dominate, with an upwelling over the sunlit hemisphere and a downwelling over the night hemisphere of the planet. Transport of oxygen and nitrogen atoms to the nightside stimulates the formation of the nitric oxide (NO) molecules, thus producing an airglow [*Mandelman et al*., 1973]. This now well-understood airglow process has been observed on Venus since the flyby of Mariner 5 in 1967 [*Barth et al*., 1967; *Bougher et al*., 1990; *Gérard et al*., 2008; *Cox et al*., 2008]. The first identification of NO as the molecule producing the airglow was made with the International Ultraviolet Explorer (IUE) by *Feldman et al*. [1979] and with Pioneer as well [*Stewart et al*., 1979; *Stewart and Barth*, 1979; *Gérard et al*., 1981]. Lately, Venus Express also recorded multiple observations of the NO Venusian nightglow. NO, as a tracer of the descending branch of the SSAS circulation, is an important molecule to study to further constrain dynamical models of the upper atmosphere of Venus.

Analyses derived from the Venus Express data [*Gérard et al*., 2008; *Royer et al*., 2010; *Stiepen et al*., 2012] have shown that the NO emission peaks at a mean altitude of 113 km, with the NO airglow being observed in the 95 to 132 km range. The limb brightness was found to range between 5 kR and 540 kR and the scale height to be about 8 km. All past observations demonstrated that the morphology and intensity of the NO airglow are highly variable on the scale of an Earth day. Nevertheless, in the case of an ideal SSAS circulation pattern, the NO airglow, as well as the O_2 airglow peaking at slightly lower altitude, are expected to maximize around midnight solar local time, since those two airglows are supposed to be tracers of the descending branch of the SSAS circulation. In fact, the observations tell a different story: since the Pioneer times a permanent spot of enhanced NO airglow emission peaking near 2 A.M. solar local time, toward the south of the equator is observed, and while the O_2 airglow peaks at midnight. Various explanations to this offset from the antisolar point are given to date. On short timescale of about 10 Earth day and less, the thermospheric Venusian circulation is overall spatially and temporally irregular, with mostly rapid changes. The Venus Thermospheric General Circulation Model (VTGCM) simulation detailed in *Brecht et al*. [2011] shows that eddy diffusion dominates the peak emission region of O_2 and NO nightglow. From statistical average of observations of the O_2 infrared (IR) nightglow, the NO UV nightglow, and nightside temperatures, they deduce the presence of a weak retrograde superrotation zonal flow (RSZ) from about 80 to 110 km and of the emergence of modest RSZ winds above 110 km. Their sensitivity test on the nightside eddy diffusion coefficient and on the wave drag term identified possible mechanisms to explain the observed noncorrelation of the two nightglows. However, the variability of the NO nightglow is still not well understood and thus long-term permanent features, such as the bright

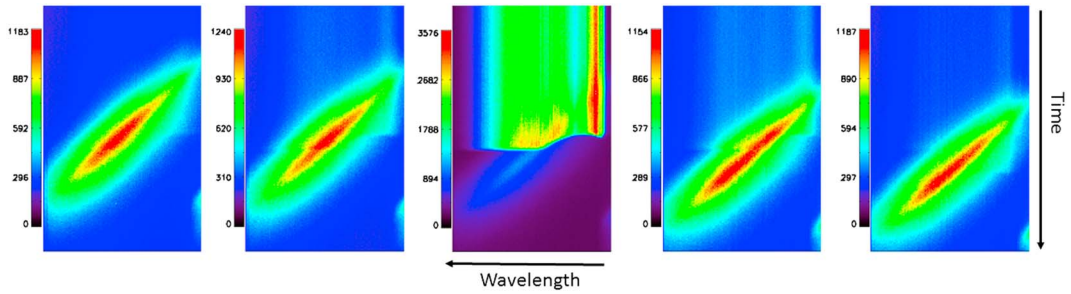

Figure 1. Example of representation of the five SPICAV bands. The color scale represents the intensity of the emission in Analogue-to-Digital Units (ADU). Each band is a tempo spectrum, with the wavelength on the *x* axis and the time on the *y* axis. The star signal is mainly visible on the central band. The red vertical line is the Lyman alpha stellar emission. An airglow—lenticular shape—is visible on every band.

patches of NO and O_2 at 2 A.M. and midnight solar local time, respectively, keep challenging our understanding of the Venus upper atmospheric dynamics [*Gérard et al*., 2009].

In this paper, we present a NO airglow model based on the inversion of the Venus Express stellar occultation data. This work revisits the paper of *Royer et al*. [2010] where a forward model of the same airglow based on the same data set was presented. The inverse model allows for a more realistic representation of the NO layer by discarding some assumptions of the forward model such as spherical symmetry and Chapman layer. It also gives access to a new parameter, which links the vertical profile shape to the spatial heterogeneity of the emissive layer.

2. SPICAV Data Set

The technique to retrieve the NO signal from the Spectroscopy for Investigation of Characteristics of the Atmosphere of Venus (SPICAV) stellar occultation data set is described in details in *Royer et al*. [2010] and *Royer* [2011]. We summarize it in this section.

For reason of telemetry limitations, the 288 spatial lines of the SPICAV instrument are binned into 5 bands, each band containing 16 or 32 lines in the case of stellar occultations. No slit is used in front of the spectrometer, thus resulting in a degradation of the spectral resolution and a convolution of the airglow signal [*Bertaux et al*., 2006a, 2006b; *Montmessin et al*., 2006 and *Villard*, 2008]. Airglow measurements do not allow for an accurate retrieving of information on the atmospheric transmission in their presence.

Because the star is a point source, its spectral structure is preserved and its signal is observed on the central band, slightly spreading to the adjacent bands. However, the airglow contribution comes as an extended source inside the atmosphere of Venus, and the removal of the slit results in the lenticular shapes superimposed on the occultation signal, as observed on tempo spectra from Figure 1. To extract the airglow signal, we use the four adjacent bands (excluding the central band), where the airglow signal is dominant and the star signal is minimal. We produce a model of light from those adjacent bands and subtract it on the central band to simulate the airglow signal [*Royer et al*., 2010]. We assume an initial atmospheric transmission to estimate the contribution of the star for each band and to calculate a mean airglow signal from the adjacent bands. This procedure is iterative. The final step consists in subtracting the modeled stellar contribution from the adjacent bands to isolate the airglow signal.

In this work, we use the airglow by-product signal as our main data set of NO emissions. We used a subset of the data set from 2006 to 2010, representing solar minimum conditions, analyzing a total of 180 observations.

3. Algorithm of Inversion

The development of the inversion method presented in this paper has been motivated by the difficulties encountered with the forward model of *Royer et al*. [2010]. In particular, some observations are not spherically symmetrical along the line of sight, due to the high spatial variability of the airglow morphology.

The forward model consisted in a simulation of the signal collected by the CCD bands of SPICAV in the case of an NO nightglow emission seen in the stellar occultation mode. It explicitly recreated each transformation

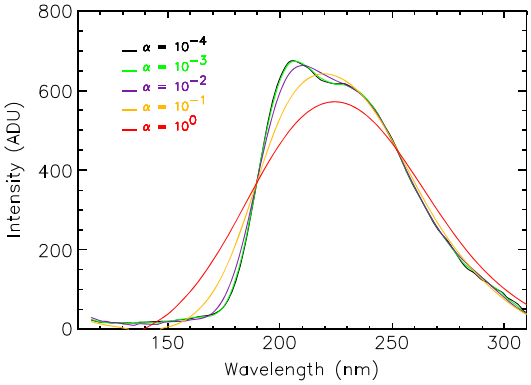

Figure 2. Effect of the Tikhonov regularization. Variation of the simulated NO spectrum as a function of the α parameter. The greater the α value, the smoother the convolved spectrum.

occurring in the optical system of the instrument. A spectrally resolved spectrum of NO obtained by SPICAV (with the slit in front of the spectrometer) during orbit 516 was used as an input to the model. The following assumptions were made: (1) the NO vertical profile of emissivity was represented by a Chapman function and integrated along the line of sight, and (2) we assumed a spherical symmetry.

The inversion method used here allows overriding those initial assumptions. In addition, the inversion algorithm has the advantage to retrieve, among others, the exact same parameters as in the forward model: a limb profile as it would be observed by SPICAV if it had an excellent spatial resolution, as well as the airglow brightness and the scale height of the NO layer. Nevertheless, the shape of the limb profile of NO is not imposed during the inversion. A linear operator is used to represent the transformation from the integrated limb profile of NO to the signal received in Analogue-to-Digital Units (ADU). The related matrix [**E**] can directly be inverted, provided some smoothing is applied. As inputs to the inverse method, we only need an NO spectrum of reference (the same as used in the forward model) to build [***E***], a NO observed spectrum with its associated geometry and the instrument parameters. The core of the model is a matrix inversion that we adjust with a Tikhonov regularization [*Tikhonov and Arsenin*, 1977; *Twoney*, 1977]. The inversion problem in our case is not well posed, the matrix [***E***] being ill-conditioned

$$\mathbf{o} = \mathbf{E} \cdot \mathbf{b} \tag{1}$$

where **o** and **b**, defined for the same altitude grid, are the observed NO spectrum and a vector containing the sought emission brightness respectively. [**E**] is a transfer matrix expressing the relation between the observed NO spectrum **o** and its vertical distribution **b**. It represents the effect of the point spread function (PSF) and of the diffraction grating on the image created on SPICAV's detector. [**E**] is a square matrix of dimension 288×288.

Knowing **o** and [**E**], we want to determine **b**. In most cases, the results obtained from equation (1) show an amplification of the noise in the observed NO spectrum. To attenuate this effect, we use the regularization of Tikhonov, introducing a constraint of smoothing which will decrease the effect of the noise in the derived brightness **b**. In order to favor a particular and relevant solution, a term of regularization is introduced in the minimization:

$$\|\boldsymbol{E} \,.\, \boldsymbol{b}\text{–}\mathbf{o}\|^2 + \|\alpha\, \Gamma \mathbf{b}\|^2 \tag{2}$$

where $[\Gamma]$ is the regularization matrix, optimized by a coefficient α to adjust the smoothing. The vector **b** being best represented by a continuous function, we choose an operator of second derivative to represent $[\Gamma]$, where h is the distance between two consecutive layers. Each layer being separated by 1 km, $(1/h)^2 = 1\ \mathrm{km}^{-2}$.

$$[\Gamma] = 1/h^2 \begin{vmatrix} -1 & 2 & 0 & 0 & \dots & 0 \\ 1 & -2 & 1 & 0 & \dots & 0 \\ 0 & 1 & -2 & 1 & \dots & 0 \\ \dots & \dots & \dots & \dots & \dots & \dots \\ 0 & \dots & 0 & 1 & -2 & 1 \\ 0 & \dots & 0 & 0 & 1 & -1 \end{vmatrix}$$

The numerical solution (the estimator of the brightness $\widehat{\boldsymbol{b}}$), is given by

$$\widehat{\boldsymbol{b}} = \left([E]^T[E] + \alpha[\Gamma]^T[\Gamma]^{-1}\right).[E]^T\boldsymbol{o} \tag{3}$$

Figures 2 and 3 demonstrate the effect of the regularization on the modeled NO spectrum and the integrated limb profile of NO. Choosing the value of the α parameter is a compromise between the overall shape of the vertical distribution, its smoothing aspect, and the shape of the inverted spectrum, which must be as close as

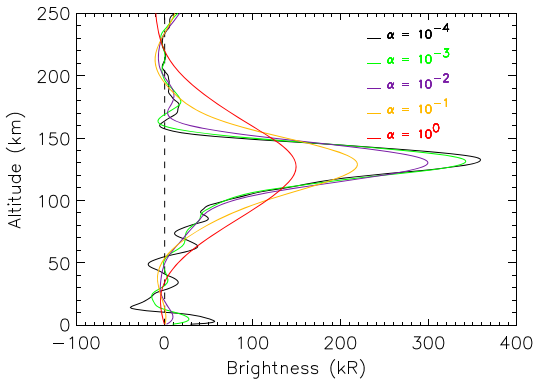

Figure 3. Effect of the Tikhonov regularization. Variation of the simulated NO limb profile, retrieved from the NO spectra of Figure 2, as a function of the α parameter.

possible to the observed spectrum. We do not assume a spherical symmetry during the inversion to retrieve the brightness integrated along the line of sight. One can notice that the greater the α value, the smoother the profile and the NO spectrum.

The inversion is more accurate than for a forward modeling approach to access the limb profile of NO. Conversely, the smoothing degrades the vertical resolution on the order of $\alpha^{1/2}$, increasing the uncertainties for the altitude of the peak of emission even if the inversion gives a more realistic shape to the vertical distribution of NO. This leads to larger relative uncertainties in the altitude of the emission peak and scale height of about 15%, while they are of about 10% for the forward model.

A horizontal length scale of the emission can also be retrieved from the inversion. Images of the field of view at a given instant *t* are thus created as seen in Figure 4. This is an example of a second airglow present in the foreground in the field of view. The horizontal distance gives information about the heterogeneity of the emissive layer and demonstrates that the NO airglow is clearly spatially variable at a constant altitude level. The horizontal distance is calculated from the latitude and longitude of the location observed on Venus. It measures the distance, as a straight line, which separate a point in the field of view from another [*Sinnott*, 1984]. The inversion method allows for exploiting the imaging capability of SPICAV. This a powerful tool to assess the spatial homogeneity of the NO emission in the field of view.

4. Results

In this section, we present the case of a nonspherically symmetric airglow with a zone of second emission visible in the field of view (observation 0267A10). The forward model struggles to reproduce this kind of airglow morphology, because of the assumption of a spherical symmetry, which results in an underestimation of the airglow brightness below a certain altitude, as seen in Figure 5.

To fully understand the modeling process, we need to keep in mind that because we do not use the spectrometer slit, the wavelength axis can also be translated into an altitude axis. For the particular observation given here, the spectral region shortward 200 nm corresponds to altitudes less than 80 km. The inverse model (Figure 5b) is able to reproduce the spectral shape of the NO spectrum as seen by SPICAV, while the forward model (Figure 5a) clearly underestimates the necessary amount of NO to reproduce the data. The forward model, because of the Chapman function, is unable to produce NO at the necessary tangent altitudes.

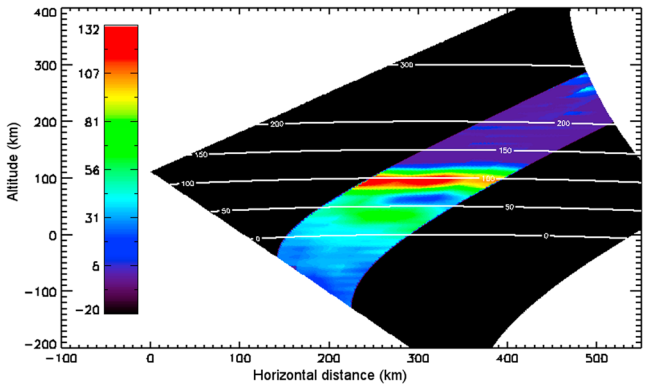

Figure 4. Image of the field of view created by the inversion algorithm for orbit 0267A10. A second emission zone is visible at tangent altitudes below the main airglow emission. The color bar expresses the airglow intensity in kR. The black color (value of −20) indicates a lack of data.

Figure 4 is an image of the field of view, created from the inversion results. A second fainter zone of NO emission is clearly visible at tangent altitude below 50 km, in the foreground or background of the main emission, all emissions being physically located around 115 km of altitude above Venus' surface. The tangent altitude

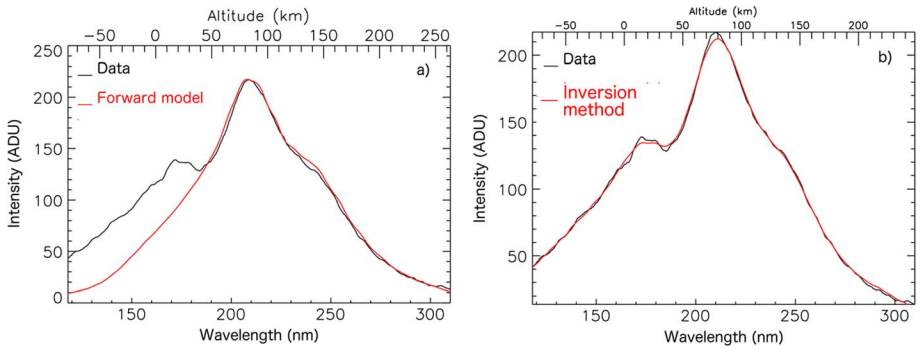

Figure 5. Best fits for observation 0267A10. (a) Best fits for the forward model of *Royer et al.* [2010]. (b) Best fit from the inversion method.

results from the distance and movement of the SPICAV instrument relative to the Venusian atmosphere, as the spectrometer scans the planet during the observation. We take into account this parallax effect to retrieve the physical altitude of each NO emission. As a consequence, an NO emission physically located around 115 km seen in the foreground/background of another emission due to the curvature of the atmosphere will appear to have a tangent altitude below 115 km. Figure 13 in *Royer et al.* [2010] illustrates the different geometries and their associated vertical distributions of the NO airglow as seen in stellar occultation mode.

Figure 6 demonstrates that by not restricting the limb profile to a Chapman layer, we are able to reproduce a realistic vertical distribution of NO, as seen from SPICAV. In addition, one can notice that the inversion method, compare to the forward model, has a tendency to lower the peak of the main emission. This is a consequence of the regularization, which decreases the vertical resolution.

The second emission zone airglow morphology is present in roughly 40% of the data set. Furthermore, this inverse model is capable to reproduce morphologies where the NO airglow is attenuated in the foreground/background as well. Those two morphologies account for about 60% of the observations contained in the SPICAV data set, which demonstrates the advantage of the inversion algorithm over the forward modeling.

Figures 7 and 8 summarize the results obtained from the inversion algorithm for all NO airglow SPICAV observations obtained between 2006 and 2010. Figure 7 shows the altitude of the NO emission peak, while Figure 8 shows the corresponding brightness. In Figure 7, the altitude of the emission peak has been statistically adjusted, as a function of the α Tikhonov coefficient, to match those of the forward model. We observe that the NO airglow peaks around 114 km. The peak of emission has the highest values near the equator, within approximately 10° of latitude, suggesting the NO airglow peak at higher altitude around the equator. Nevertheless, we do not observe a clear trend between the latitude and the peak altitude: the lowest altitudes of the emission peak occur between 50°S and 60 N of latitude. But only the highest altitudes (up to 140 km) are found around the equator. In addition, no correlation between the altitude of the emission peak and the solar local time is observed.

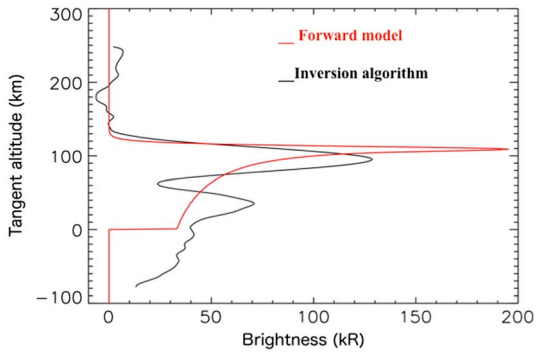

Figure 6. Vertical profile for observation 0267A10 for both, the forward model and the inversion algorithm.

In Figure 8, the brightness of the emission at the peak shows a concentration of large values at about 2 A.M. solar local time (between 01:00 and 03:00 A.M.) and south of the equator. Airglows are enhanced by about a factor of 4 relative to the average brightness. This observation based on SPICAV data is similar to observations made by the Pioneer/PV-OUVS instrument [*Stewart et al.*, 1980]. They were the first to observe a bright spot of NO airglow located south of the equator around 2 A.M. solar local time. This result has since been confirmed by *Bougher et al.* [1990] and by *Stiepen et al.* [2013], with the

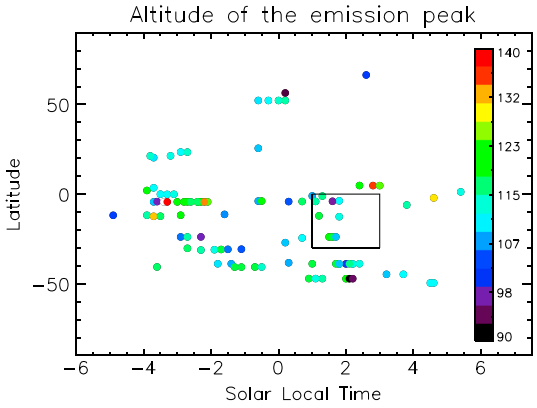

Figure 7. Altitude of the peak of the NO emission in kilometer, retrieved from the inversion algorithm. The square represents the region where Pioneer Venus observed the enhanced spot. The altitude of the emission peak is expressed in kilometers.

SPICAV nadir observations. The map compiled by *Stiepen et al.* [2013] contains data for low to medium solar activity. *Stewart et al.* [1980] data were for solar maximum conditions. Given the 30 years separating the two sets of observations, we can thus conclude that the region of enhanced NO emission has been observed multiple times, with different instruments and geometries, over different solar conditions, suggesting that this is a long-term permanent feature of the Venusian upper atmosphere. This is an interesting result given the high temporal and spatial variability of the NO airglow on short timescale of 10 Earth days or less.

5. Discussion

More SPICAV images of the Venusian NO airglow layer are available in the supporting information. They demonstrate the highly variable morphology of the airglow. The spatial horizontal homogeneity over a constant altitude level usually spans several hundreds kilometers. Thus, the NO airglow can cover a large portion of the Venus sky at a given altitude. Frequent secondary NO emissions are seen at tangent altitudes lower than the main airglow layer, revealing the patchiness of the emission. No correlation between the morphology and the intensity of the airglow is observed.

Results from previous studies and this work are summarized in Table 1. *Gérard et al.* [2008] published the first SPICAV results, based on 201 limb observations. The stellar occultation data set analyzed in this work benefits from a more homogeneous distribution of the data in latitude and longitude, as well as in solar local time. The data set from *Gérard et al.* [2008] lacks measurements between 22 h and midnight solar local time and uses measurements exclusively made in the Northern Hemisphere. The stellar occultation set contains more data for the Southern Hemisphere. Both data sets are thus complementary. In 2012, *Stiepen et al.* [2012] published results from a statistical study of the NO airglow based on a larger data set for the Northern Hemisphere from *Gérard et al.* [2008]. A second study from *Stiepen et al.* [2013] focused on nadir observations made by SPICAV. They published the first map of ultraviolet NO Venus nightglow since the Pioneer Venus era for low solar activity (from 2006 to end of 2010), among others, and possess a spatial coverage equivalent to this study. Results are compiled in Table 1.

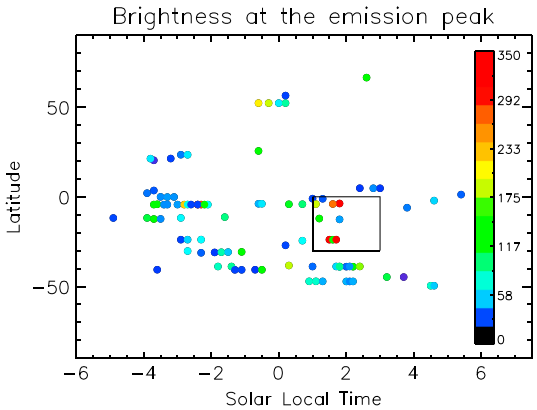

Figure 8. Brightness map of the peak of the NO emission, retrieved from the inverse model. The square represents where Pioneer Venus saw the enhanced spot. The brightness is expressed in kR.

In the case of an ideal SSAS circulation pattern, both O_2 and NO emissions are expected to peak around midnight solar local time, since those two airglows are believed to be tracers of the descending branch of the SSAS circulation occurring in the upper atmosphere of Venus.

Multiple attempts have been made to explain the lack of correlation observed between the O_2 and NO emissions. VTGCM simulations and sensitivity tests realized by *Brecht et al.* [2011] show that two circulation patterns may coexist in the upper atmosphere: below 70 km of altitude, the Venusian atmosphere is dominated by the retrograde superrotating zonal flow, and the SSAS circulation

Table 1. Summary of Results of the Characteristics of the Venusian NO Layer From This Work (Inversion Method) and Earlier NO Airglow Models and Observations

Parameters	*Gérard et al.* [2008]	*Royer et al.* [2010] Forward Model	*Stiepen et al.* [2012]	This Work Inversion Method
Peak altitude of limb profile	112.6 ± 5.8 km	114.5 ± 7.7 km	115.5 ± 7 km	114.0 ± 10 km
Scale height of NO layer	7 km	8.2 ± 3.1 km	----	20.0 ± 10 km
Mean intensity of airglow	~55 kR	From 10 kR to 200 kR	60 kR	59.3 ± 63 kR

becomes dominant only above 120 km of altitude. Between 70 and 120 km, where the O_2 and NO airglows occur, is a region of transition, where the two major flow patterns cited above are presumed to be superimposed. *Brecht et al.* [2011] demonstrate that the eddy diffusion mostly controls the altitude of the nightglow peak, while the nightglow intensities are strongly impacted by winds. It is important to recognize that the wave drag parameter use in the VTGCM is a proxy for the RSZ wind velocity. The wind sensitivity test they performed is related to the wave drag parameter, which is part of the Rayleigh friction and implemented to approximate gravity wave momentum drag effects. This reinforces the fact that gravity wave momentum deposition around 110–115 km is regularly proposed to explain the discrepancy between the O_2 and NO regions of enhanced emission [*Brecht et al.*, 2011].

SPICAV images can help investigate wave pattern seen in the airglow, through a systematic measurement of the horizontal homogeneity of the NO layer. The inverse model presented here is a powerful tool to investigate the short timescale variability of the NO airglow as well. Temporal evolution of the airglow can be studied with a further analysis, by building field-of-view images at each step of the stellar occultation.

6. Conclusion

Using the imagery capabilities of the SPICAV instrument, we are able to give a first quantification of the horizontal extent of the NO layer present in the atmosphere of Venus. Results reveal a very complex dynamics, where rapid short-time changes are superimposed on a more stable permanent feature observed for decades. Monitoring of the airglow long-term patterns in the atmosphere of Venus will bring additional constraints to be implemented in dynamical models and a better understanding of such atmospheres with a superrotation regime.

Acknowledgments
This research was funded by a grant from the French Ministry for Research (MENRT funds) and by the Center for National Scientific Research (CNRS). This work is also supported by the Venus Express mission. All data are publicly available on the Venus Express Planetary Science Archive of the European Space Agency. The authors thank Jean-Loup Bertaux for giving access to the SPICAV data and providing some sources code for the analysis.

References

Barth, C. A., J. B. Pearce, K. K. Kelly, L. Wallace, and W. G. Fastie (1967), Ultraviolet emissions observed near Venus from Mariner V, *Science*, *158*, 1675–1678.

Bertaux, J.-L., et al. (2006a), SPICAM on Mars Express: Observing modes and overview of UV spectrometer data and scientific results, *J. Geophys. Res.*, *111*, E10S90, doi:10.1029/2006JE002690.

Bertaux, J.-L., et al. (2006b), SPICAV on Venus Express: Three spectrometers to study the global structure and composition of the Venus atmosphere, *Planet. Space Sci.*, doi:10.1016/j.pss.2007.01.016.

Bougher, S. W., J.-C. Gérard, A. I. F. Stewart, and C. G. Fessen (1990), The Venus nitric oxide night airglow: Model calculations based on the Venus thermospheric general circulation model, *J. Geophys. Res.*, *95*, 6271–6284.

Brecht, A. S., S. W. Bougher, J. C. Gerard, C. D. Parkinson, S. Rafkin, and B. Foster (2011), Understanding the variability of nightside temperature, NO UV and O_2 IR nightglow emissions in the Venus upper atmosphere, *J. Geophys. Res.*, *116*, E08004, doi:10.1029/2010JE003770.

Cox, C., A. Saglam, J.-C. Gérard, J. L. Bertaux, F. Gozàlez-Galindo, F. Leblanc, and A. Reberac (2008), Distribution of the ultraviolet nitric oxide Martian night airglow: Observations from Mars Express and comparisons with a one-dimensional model, *J. Geophys. Res.*, *113*, E08012, doi:10.1029/2007JE003037.

Feldman, P. D., H. W. Moos, J. T. Clarke, and A. L. Lane (1979), Identification of the UV nightglow from Venus, *Nature*, *279*, 221.

Gérard, J.-C., A. I. Stewart, and S. W. Bougher (1981), The altitude distribution of the Venus ultraviolet nightglow and implications on vertical transport, *Geophys. Res. Lett.*, *8*, 633–636.

Gérard, J.-C., C. Cox, A. Saglam, J.-L. Bertaux, E. Villard, and C. Nehmé (2008), Limb observations of the ultraviolet nitric oxide nightglow with SPICAV on board Venus Express, *J. Geophys. Res.*, *113*, E00B03, doi:10.1029/2008JE003078.

Gérard, J.-C., C. Cox, L. Soret, A. Saglam, G. Piccioni, J.-L. Bertaux, and P. Drossart (2009), Concurrent observations of the ultraviolet nitric oxide and infrared O_2 nightglow emissions with Venus Express, *J. Geophys. Res.*, 114, E00B44,, doi:10.1029/2009JE003371.

Mandelman, M., T. Carrington, and R. A. Young (1973), Predissociation and its inverse, using resonance absorption NO($C^2\Pi$) ↔ N + 0, *J. Chem. Phys.*, *58*, 84–90.

Montmessin, F., E. Quémerais, J.-L. Bertaux, O. Korablev, P. Rannou, and S. Lebonnois (2006), Stellar occultations at UV wavelength by the SPICAM instrument: Retrieval and analysis of Martian haze profiles, *J. Geophys. Res.*, *111*, E09S09, doi:10.1029/2005JE002662.

Royer, E. (2011), Etude des emissions de monoxide d'azote (NO) observées en ultraviolet par SPICAV/Venus Express en mode d'occultation stellaire, PhD Thesis Université Pierre et Marie Curie

Royer, E., F. Montmessin, and J.-L. Bertaux (2010), NO emissions as observed by SPICAV during stellar occultations, *Planet. Space Sci.*, *58*, 1314–1326, doi:10.1016/j.pss.2010.05.015.

Sinnott, R. W. (1984), Virtues of the Haversine, *Sky and Telescope*, *62*, 159.

Stewart, A. I., and C. A. Barth (1979), Ultraviolet night airglow of Venus, *Science*, *205*, 59.

Stewart, A. I. F., J.-C. Gérard, D. W. Rusch, and S. W. Bougher (1980), Morphology of the Venus ultraviolet night airglow, *J. Geophys. Res.*, *85*, 7861–7870.

Stewart, A. I., D. E. Anderson Jr., L. W. Esposito, and C. A. Barth (1979), Ultraviolet spectroscopy of Venus: Initial results from the Pioneer Venus Orbiter, *Science*, *203*, 777–779.

Stiepen, A., L. Sorret, J. C. Gerard, C. Cox, and J. L. Bertaux (2012), The vertical distribution of the Venus NO nightglow: Limb profiles inversion and one-dimension modeling, *Icarus*, *220*, doi:10.1016/j.icarus.2012.06.029.

Stiepen, A., J. C. Gerard, M. Dumont, C. Cox, and J. L. Bertaux (2013), Venus nitric oxide nightglow mapping from SPICAV nadir observations, *Icarus*, *226*, doi:10.1016/j.icarus.2013.05.031.

Tikhonov, A. N., and V. Y. Arsenin (1977), *Solution of Ill-Posed Problems*, V.H. Winston, Washington, D. C.

Twoney, S. (1977), *Some Aspects of the Inversion Problem in Remote Sensing, Inversion Methods in Atmospheric Remote Sensing*, pp. 41–65 , NASA Langley Res. Center, Hampton, Va.

Villard, E. (2008), L'instrument SPICAV d'étude de l'atmosphère de Vénus sur la mission Venus Express: Caractérisation instrumentale et observation en vol, PhD Thesis Université Versailles Saint-Quentinn-En-Yvelines.